Microstructure-oxidation resistance relationship in Ti3AlC2 MAX phase

E. Drouelle, V. Gauthier-Brunet, J. Cormier, P. Villechaise, P. Sallot, F. Naimi, F. Bernard, S. Dubois

Version of Record: https://www.sciencedirect.com/science/article/pii/S0925838820304254
Manuscript_8d2e73e9a99e43baf7d9a76bdb70e04a

Microstructure-oxidation resistance relationship in Ti_3AlC_2 MAX Phase

E. Drouelle[1, 2], V. Brunet[1], J. Cormier[1], P. Villechaise[1], P. Sallot[2], F. Naimi[3], F. Bernard[3], and S. Dubois[1]

[1] Institut PPRIME, CNRS/Université de Poitiers/ENSMA, UPR 3346, Boulevard M. et P. Curie, TSA 41123, 86073 Poitiers Cedex 9, France.

[2] Safran Tech, 1 rue Geneviève Aubé, CS 80112, 78772 Magny les hameaux Cedex, France

[3] Laboratoire Interdisciplinaire Carnot de Bourgogne, UMR 6303 CNRS-Université de Bourgogne Franche-Comté, 9 Av. Alain Savary, BP 47870, 21078 Dijon Cedex, France

Abstract

Spark Plasma Sintering and Hot Isostatic Pressing were used to synthesize coarse-grained and fine-grained Ti_3AlC_2 specimens. Moreover, Spark Plasma Sintering processing parameters were modified in order to vary the TiC, Al_2O_3 and Ti_xAl_y impurity and the porosity contents in the fine-grained samples. The influence of the Ti_3AlC_2 microstructure on the oxidation resistance was assesed. It is demonstrated that the grain size can drastically modify the oxidation resistance. The higher density of grain boundaries, in fine-grained specimens, increases the number of Al diffusion paths and leads to the formation of a protective alumina scale. In coarse-grained sample, Al diffusion is the rate limiting step of the α–Al_2O_3 formation and TiO_2 is formed simultaneously to alumina. TiC impurities and porosity are demonstrated to be detrimental to the oxidation resistance in the 800°C – 1000°C temperature range by favouring TiO_2 formation. Finally, it is also shown that, for fine-grained specimens, the oxide scale grows very slowly for oxidation times in the range 20-40 days.

1. Introduction

MAX phase materials are quite recent materials developed nearly 50 years ago by Nowotny [1, 2]. These ternary nano-layered compounds can be described by the empirical formula $M_{n+1}AX_n$, with n equal to 1, 2 or 3, where M represents an early transition metal, A represents A-group elements (i.e.: from columns IIIA to VIA of the periodic table) and X represents carbon and/or nitrogen. The hexagonal structure (P63/mmc) of MAX phase materials is characterized by M_6X octahedra separated by A atomic layers. This structure, combining both strong covalent M-X bonds and weaker M-A bonds, confers to MAX phases properties of both ceramics and metals. Like ceramics, they are stiff, lightweight, chemically stable and oxidation resistant. Like metals, they are relatively ductile at high temperature, machinable, resistant to thermal shock and they exhibit good electric and thermal conductivity. This class of materials, and more specifically Cr_2AlC, has also been used as a coating for Ni-based polycrystalline superalloy [3, 4], taking advantage of its very good corrosion/oxidation resistance [5].

Given their relatively low density and their ability to resist high temperatures, these materials are good candidates for high temperature structural applications such as vanes, shrouds, or even blades for gas turbine applications [6]. Indeed, even if they have intrinsic lower creep resistance compared to widely evaluated cast Ni-based superalloys for such kind of components, their specific mechanical properties (i.e. taking into consideration material's density), especially in creep [7-10], may be interesting for the design of more efficient gas turbine, by achieving lighter and/or more refractory (rotating) components. Various papers [11-29] have investigated the oxidation resistance of different MAX phases (containing Al as A element) in the 900°C - 1300°C temperature range. Even if the oxidation mechanisms and oxidation kinetics are still open to prove (are oxidation kinetics cubic or parabolic? [24]), most cases demonstrate the formation of alumina scales up to hundreds of hours. This is due to the

fact that aluminum activity in this temperature range is strong enough to favour alumina formation. Only one paper attempted to investigate the oxidation resistance of various MAX phases in gas turbine environment [6] for long term durations (i.e. up to 2,500 h). It was shown a good stability and oxidation resistance at 1150°C of Ti_2AlC (if not Al-depleted or damaged [30]) in comparison to Cr_2AlC in simulated gas turbine environment, leading to a better adhesion of a thermal barrier coating deposited onto these materials. Concerning the short-term (cumulative time=29h) environmental resistance of Cr_2AlC at 1200°C under thermal gradient loading using a burner rig, Gonzalez-Julian and co-workers reported the formation of a protective and adherent α-Al_2O_3 layer to the Cr_2AlC substrate [31].

In many industrial applications, thermal transients are of great importance and studying oxidation resistance of materials in lower temperature range is critical to assess, to be sure that the transition regimes between oxide scales are not detrimental to the lifetime of the parts. Actually, to the authors' knowledge, the absence of consensus on the oxidation resistance in MAX phase systems may result from microstructure differences (e.g. grain size, secondary phases …) that may affect the oxidation mechanisms. Indeed, relationships between processing parameters, resulting microstructure and oxidation resistance have not been sufficiently documented in previous literature [11-34]. The main goal of the present paper is to establish such kind of relationship(s) for Ti_3AlC_2 in the critical temperature range 800-1000°C, where the material is the most susceptible to modification in oxide scales, and more particularly for long exposure times (up to 1,000 h).

2. Material and methods

Highly dense Ti_3AlC_2 samples were synthesized by powder metallurgy, using two methods: the densification of Ti_3AlC_2 powders using Spark Plasma Sintering (SPS) technique and, the

simultaneous synthesis and densification of Ti_3AlC_2 using Hot Isostatic Pressing (HIPing) process. The objective was to produce dense Ti_3AlC_2 bulk samples with different microstructures (coarse-grained for HIP and fine-grained for SPS) to study, among other parameters (porosity and secondary phases), grain size influence onto the oxidation resistance over the temperature range 800-1000°C.

To synthesize SPSed samples, titanium (Alfa Aesar, 99.5%, 150-250 µm), aluminum (Alfa Aesar, 99.5%, 45-150 µm) and titanium carbide (Alfa Aesar, 99.5%, 2 µm) powders were blended in quasi stoichiometric proportions (i.e. Ti-1.05Al-1.9TiC and Ti-Al-1.9TiC) for 20 min in a Turbula® mixer. The reactant powder mixture was encapsulated in a glass container in primary vacuum and then, sintered in argon atmosphere during 2 h at 1450°C to produce a highly porous Ti_3AlC_2 bulk material. The porous material was then crushed into Ti_3AlC_2 powder (mean particle size centered around 15µm from laser granulometry analyses). The Ti_3AlC_2 powder was subsequently densified by SPS in high vacuum for temperature, pressure and time ranging from 1200-1400°C, 30-75 MPa and 2-20 min respectively. Specimens 60 mm in diameter were produced.

The synthesis and microstructure characterization of Ti_3AlC_2 samples produced by HIPing has been described in detail elsewhere [35-37]. Briefly, to fabricate Ti_3AlC_2 samples, a Ti-Al-1.9TiC reactant mixture was firstly ball milled in a Turbula. The mixed powders were cold-compacted and the green bodies were then sealed into glass containers in vacuum and HIPed at 1450°C for 2 h total. The pressure at such a temperature was 50 MPa and was held for 1 h. After HIPing, the samples were machined to remove the glass container and sliced using a diamond saw.

X-Ray Diffraction (XRD) analyses were performed using a Bruker D501 diffractometer with Cu-Kα radiation for the identification of secondary phases contained in the bulk Ti_3AlC_2 materials

and for the identification of the oxidation products. XRD data were refined using the MAUD software in order to assess the composition of the different Ti_3AlC_2 samples. After an appropriate mechanical polishing of the Ti_3AlC_2 SPSed samples, White and circularly Polarized Light Microscopy (WPLM, Zeiss Imager Vario Z2) was used to investigate the grain size distribution and to quantify the amount of the secondary phases [38]. The microstructure of both the Ti_3AlC_2 bulk samples (grain size, distribution of pores, location and chemical composition of secondary phases) and the oxidation products (morphology and composition of the oxide scale) were examined by Scanning Electron Microscopy using a highresolution field-emission gun scanning electron microscope (FESEM, JEOL 7001F-TTLS) coupled with energy-dispersive X-ray spectrometer (EDS, Oxford Energy) for chemical analyses. The porosity content was measured using Archimedes' method using water.

To investigate isothermal oxidation behavior in the 800-1000°C temperature range, cylindrical (diameter: 6-10 mm, thickness: 0.5-2 mm) and parallelepiped (2.5 X 2.5 X 3 mm^3) specimens were low-stress polished with SiC paper up to 2400 grade prior to oxidation tests. First, oxidation tests were performed in ambient laboratory air under atmospheric pressure in a classical furnace during 1,000 h. Specimens were introduced in the furnace once the oxidation temperature was reached, and they were air-cooled outside of the hot furnace after different durations of oxidation. Second, the oxidation kinetics of Ti_3AlC_2 MAX phase compound was measured using isothermal thermogravimetric tests (Setaram Setsys TG16 and Setaram Setsys Evolution) under synthetic air (N_2-20%O_2) for 100 to 200 h. Samples were suspended in a microbalance equipped with a vertical reaction furnace. Heating and cooling were performed in synthetic air. Only kinetics recorded during the isothermal step will be presented here.

3. Results and discussion

3.1. Microstructural characterization of the Ti_3AlC_2 HIPed and SPSed samples

Powder mixtures with two different Al stoichiometries were used together with different SPS densification conditions (T, P, t) to intentionally vary the secondary phases and porosity contents. Table 1 reports the microstructural characteristics *(secondary phase content, porosity content, mean surface area of the Ti_3AlC_2 grains)* and the corresponding densification parameters of the Ti_3AlC_2 samples which will be further oxidized.

SPS parameters	Al_2O_3 + porosity vol. % from OM	TiC vol. % from OM	Ti_xAl_y vol. % from OM	porosity vol. % from Archimede's method (±0.3%)	vol. % Al_2O_3 from Rietveld refinement (±0.1%)	vol. % TiC from Rietveld refinement (±0.1%)	Mean surface area of the grains (μm^2)
1315°C/75MPa/2min Al content : 1.05	2.5-4.1	0.3-0.4	0.02-0.99	0.5-1.5	0-1.4	0.1-1.1	10-15 ±1
1330°C/60MPa/5min Al content : 1.05	3.5	0.04	0.26	1.4-7.9	0-0.3	0.8-2	7±1
1330°C/30MPa/7min Al content : 1.05	6.1	0.2	0.57	7.1-7.5	0-0.9	0-0.2	13±1
1330°C/60MPa/5min Al content : 1.00	1.4	1.0	0.61	-1.4-5.2	0-0.4	2-11	17±2

Table 1: (Alumina+porosity) vol. %, TiC vol. % and Ti_xAl_y vol. % deduced from White Light and Polarized Light Microscopy – Porosity content determined from Archimede's method, alumina and TiC vol. % determined from Rietveld refinement and mean grain surface area determined from image analysis with respect to the different SPS parameters (maximum reached temperature/maximum pressure/dwell time). An excess of Al has been used in the reactant mixture (1.9TiC+1.05Al+1.0C) except in the last experiment where Al content is 1.00.

From XRD results and SEM/EDS analyses, Ti_xAl_y intermetallic (with various x and y stoichiometries), Al_2O_3 and TiC are the main secondary phases detected after SPS treatment. Figure 1a shows a Polarized Light Microscopy observation of a SPSed polished sample surface. Figure 1b shows a White Light Microscopy observation of the same sample surface. In figure 1a and 1b, pores and Al_2O_3 impurities appear in black. TiC impurity appears as dark grey whereas Ti_xAl_y intermetallics appear as white area in figure 1b. Ti_xAl_y, Al_2O_3+porosity and TiC contents were quantified using optical microscopy. TiC and Al_2O_3 contents were also

calculated from Rietveld refinement of the XRD data. Grain size distribution and mean surface area of the grains were determined from image analyzes of the WPLM observations.

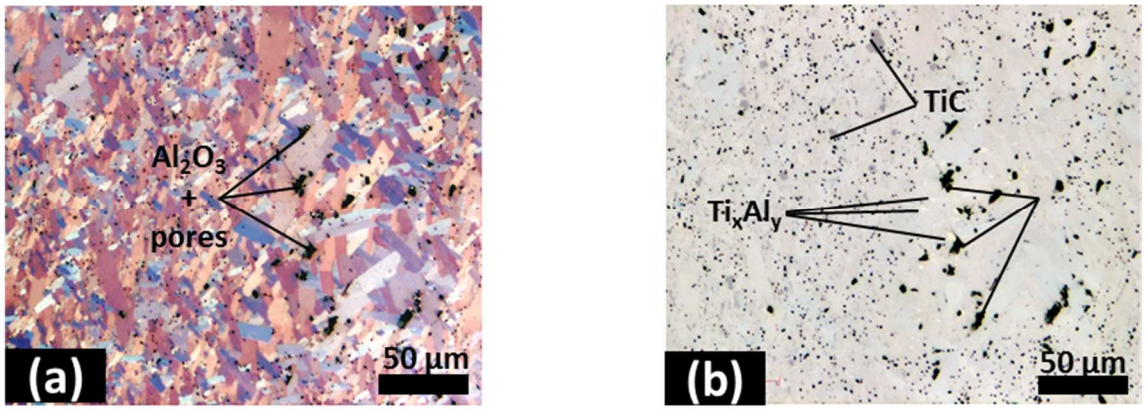

Figure 1: Polarized (a) and White (b) Light Microscopy images obtained on a SPSed sample.

A complete description of the SPS parameters' effects on microstructure characteristics is reported elsewhere [38]. The present paper only mentions some general trends regarding the impact of the powder mixture stoichiometry and the influence of the SPS parameters for the Ti_3AlC_2 samples further investigated:

- Temperature in the range 1315-1330°C does not affect the purity of the Ti_3AlC_2 end-product based on XRD results and OM analyses (see Table 1). Such a conclusion can be extended to the temperature range 1200-1400°C [38].

- Starting with Ti-1.05Al-1.9TiC powder mixture, purity is in the range 98-99 vol.%. Starting with Ti-1Al-1.9TiC mixture, TiC content increases up to 11 vol.% depending on the analyzed area of the sample (see Table 1).

- Decreasing the pressure from 75 to 30MPa involves an increase of the porosity from 1.5 to 7 vol.% (see Table 1).

For the large Ti_3AlC_2 samples produced (60 mm in diameter), for which no external heating source was used during SPS treatment, microstructural heterogeneities in terms of secondary

phase content, density and grain size were noticed after densification of the MAX phase powder. These microstructural heterogeneities may be attributed to the generation of thermal gradient when the sample diameter was increased [39]. Image analysis resulting from SEM and OM observations, have evidenced that secondary phases are not uniformly distributed in the different specimens produced. Such a result has been confirmed by the different OM and Rietveld refinement quantifications performed from samples taken in different regions of the pellet [38]. Moreover, density values are appreciably greater in the core compared to the periphery of the different samples, suggesting the existence of densification gradient between these two areas [38]. At least, PLM observations have highlighted a large grain size distribution [38]. As an example, figure 1a shows that about 50% of the grain population exhibits a surface smaller than 2 μm^2 while the mean surface area of the grains is in the range 7-17 μm^2 for the Ti_3AlC_2 samples further oxidized (see Table 1). As a consequence, in order to minimize such microstructure heterogeneities effects, small-sized Ti_3AlC_2 samples were cut and oxidized.

To further investigate the grain size effect on the oxidation properties of Ti_3AlC_2 MAX phase, coarse-grained samples were produced by HIP [35-37]. Briefly, as observed in Figure 2, HIPed samples exhibit Ti_3AlC_2 grain size which length is in the range 60-100 µm and width in the range 10-40 µm. Ti_xAl_y intermetallic compounds are sometimes located in the grain boundaries of the MAX phase.

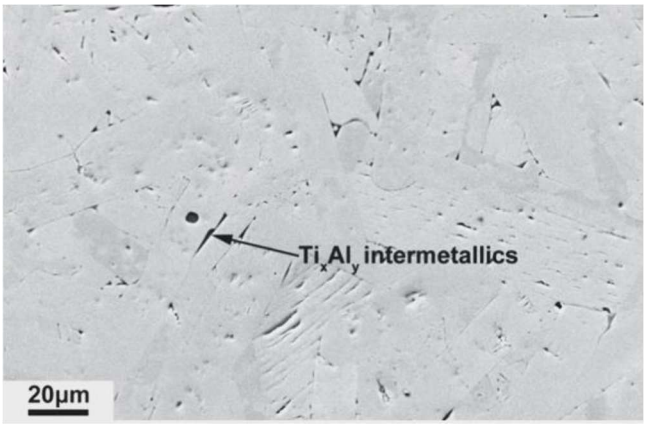

Figure 2: Scanning electron micrograph of the Ti_3AlC_2 HIPed sample surface.

3.2. Microstructural characterization of the oxidation end-products

3.2.1. Effect of the oxidation temperature

Different samples densified by SPS at 1315°C/75MPa/2min from heat treated Ti-1.05Al-1.9TiC powder mixtures were used. Oxidation tests were performed in air under atmospheric pressure, at 800, 900 and 1,000°C, in a resistive furnace during 1,000 h. These samples, placed within alumina crucibles, were removed from the furnace for different durations in order to be weighed and analyzed. Figure 3 shows the weight gain per surface unit area as a function of the oxidation time for the three investigated temperatures.

It is important to note that, for all the samples tested at the different temperatures and based on observations, the oxide layer exhibits a good adhesion with the MAX phase substrate and no spallation was detected during specimen's cooling down to room temperature.

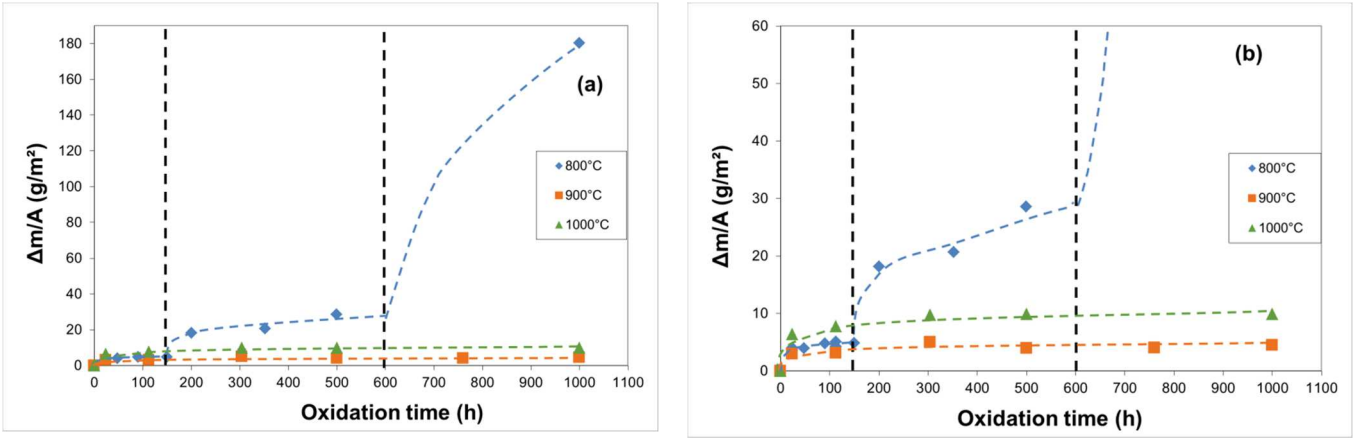

Figure 3: Oxidation tests in ambient air at 800, 900 and 1,000°C up to 1,000 h performed on different samples densified by SPS at 1315°C/75MPa/2min from heat treated Ti-1.05Al-1.9TiC powder mixtures. (a) Weight gain per surface unit area plotted as a function of the oxidation time for the three investigated temperatures, (b) magnification on the 0-60 g.m^{-2} weight gain per surface unit area.

From figure 3, three oxidation stages may be distinguished at 800°C:

- A first stage from 0 to 150 h of oxidation: the weight gain is low and reaches a first stabilization step,

- A second stage from 150 h to approximately 500 h of oxidation: it corresponds to a significant increase of the weight gain and a second stabilization step,

- A third stage starting at a time in the range 500-1000 h. The accurate oxidation duration from which this change occurs was not assessed in this study. Dotted lines in Fig. 3 are thus a guide for the eye and 600h has been randomly chosen between 500 and 1000h to represent this kinetics modification. The third stage is characterized by a high weight gain around 180 g/m^2 after 1,000 h oxidation (as compared to 5 g/m^2 and 10 g/m^2 for the samples oxidized at 900°C and 1,000°C).

XRD characterization of the oxidation products (outer surface) has been performed after 24 h, 500 h and 1,000 h of oxidation at 800°C (*not presented here*). XRD peaks of Ti_3AlC_2 phase are detected after 24 h of oxidation at 800°C. After 500 h and 1,000 h of oxidation, MAX phase is no longer detected because of the large thickness of the oxide layer. Rutile-TiO_2 is identified

whatever the oxidation time. α-Al_2O_3 is detected after 500 h of oxidation but is no longer observed after 1,000 h of oxidation. The thickness of the external TiO_2 layer (about 20 µm) is too large for the α-Al_2O_3 inner layer to be detected after 1,000 h of oxidation.

The observation of the oxidized sample surface using OM (Figure 4a) reveals the presence of a grey alumina layer with a few orange spots of TiO_2 on the periphery of the samples after 24 h of oxidation at 800°C. After 500 h and 1,000 h of oxidation at 800°C, the orange TiO_2 layer covers the whole surface of the sample; this layer exhibits a greater thickness after 1,000 h of oxidation at 800°C (about 20 µm), as also demonstrated using XRD.

X-ray mapping using EDS provides the distribution of Ti, Al, C, and O elements in the oxidized sample cross section after 24 h, 500 h and 1,000 h of oxidation at 800°C (Figure 4b). After 24 h of oxidation, EDS maps indicate the formation of both TiO_2 and Al_2O_3 equiaxed grains. Such a stacking of particles is characteristic of the MAX phase, it does not result from damage during sectioning and/or embedding. For such a short oxidation time, the fact that the alumina scale is not detected by XRD could be attributed to a very small volume fraction or to its amorphous structure, as observed in previous oxidation tests [32, 33]. Indeed, the presence of amorphous Al_2O_3 has been evidenced for Ti_3AlC_2 samples oxidized at low temperatures (lower than 700°C) [32] or during a short oxidation time, about 20 minutes, at temperature lower than 900°C [33]. After 500 h of oxidation at 800°C, different oxide layers have been identified: an external TiO_2 layer (layer C), an intermediate layer enriched in Al_2O_3 (layer B) and an internal layer in contact with the MAX phase containing both TiO_2 and Al_2O_3 (layer A). Pores are observed at the interface between layers B and C. Such a microstructure of the oxide scale is in good agreement with previously published results on Ti_3AlC_2 phase [11-17]. After 1,000 h of oxidation at 800°C, the structure of the different oxide layers is similar to the ones observed

after 500 h of oxidation. Nevertheless, layer A exhibits well-organized alternative lamellas of Al_2O_3 and TiO_2, TiO_2 being the main oxide. Carbon is detected into the whole oxide layer after 500 h of oxidation and it appears more concentrated into the intermediate Al_2O_3 layer (layer B) after 1,000 h of oxidation.

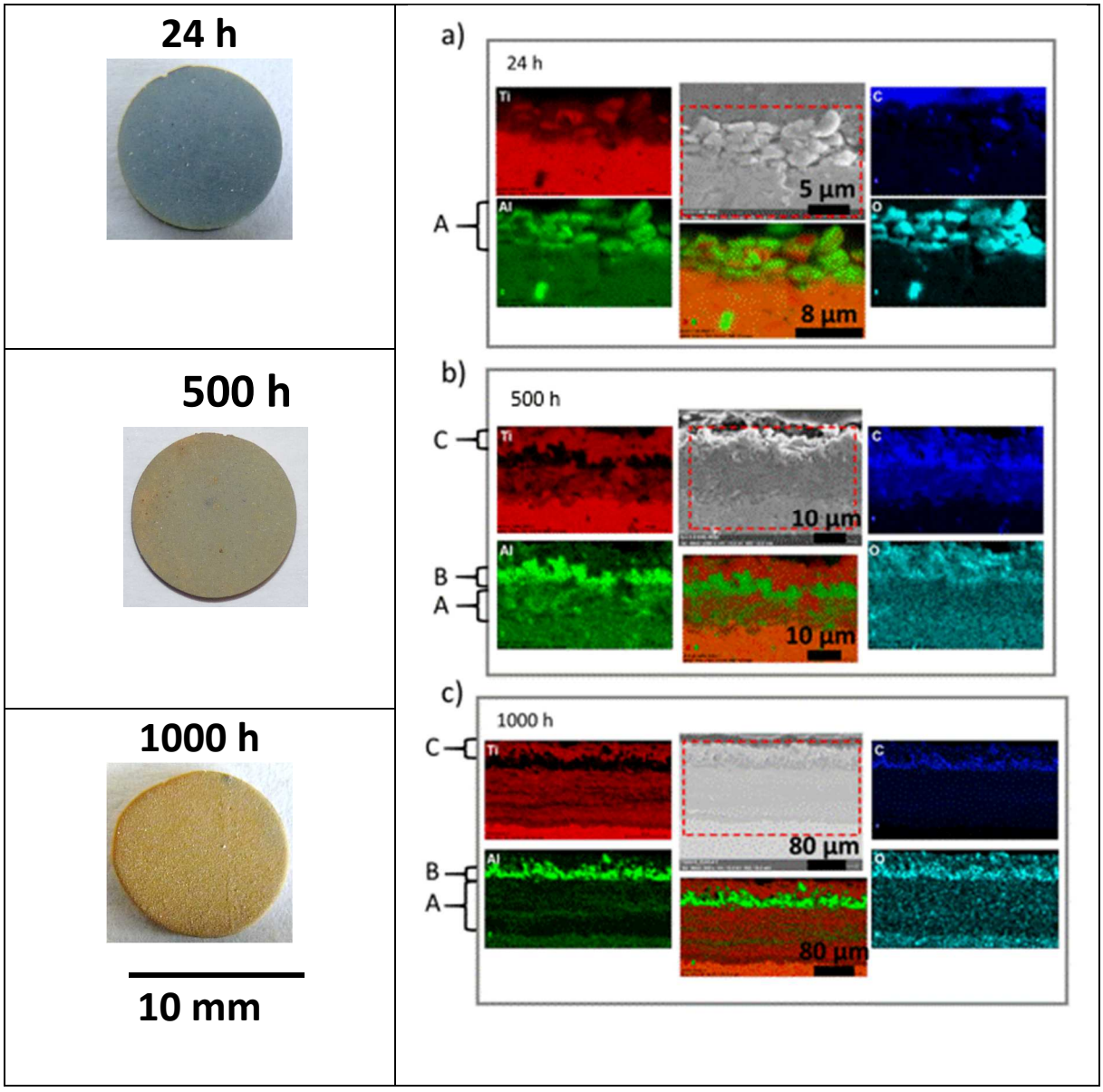

Figure 4: Oxidation tests in ambient air at 800°C up to 1,000 h performed on different samples densified by SPS at 1315°C/75MPa/2min from heat treated Ti-1.05Al-1.9TiC powder mixtures. On the left, White Light microscopy images of the sample surface oxidized during 24 h, 500 h and 1,000 h at 800°C. On the right, scanning electron microscopy cross section observation and Ti, Al, C and O corresponding X-Ray maps of the oxide scale after oxidation during 24 h (a), 500 h (b) and 1,000 h (c) at 800°C in ambient air.

As reported in Figure 3, after 300 h of oxidation at 900 and 1,000°C, weight gain reaches a plateau, the weight gain being higher at 1,000°C.

After 24 h and 1,000 h of oxidation at 900 and 1000°C, Ti_3AlC_2, TiO_2 rutile and α-Al_2O_3 phases are detected by XRD (*not presented here*). The intensity of the α-Al_2O_3 XRD peaks increases after 1,000 h of oxidation which indicates the growth of such a protective oxide during the thermal treatments at 900 and 1,000°C. Furthermore, the presence of MAX phase XRD peaks whatever the oxidation time at such temperatures demonstrates that the oxide layer remains quite thin, as confirmed from SEM observations (Figure 5).

After 24 h and 1,000 h of oxidation at 1,000°C, the surface of the samples examined using OM show a similar aspect: some TiO_2 nodules are present at the surface of the grey Al_2O_3 layer (Figure 5a). The slow weight gain reported in Figure 3 is thus in good agreement with the morphology of the oxide layer during thermal treatment.

X-ray mapping using EDS provides images of Ti, Al, C and O elements distributions in the oxidized sample cross section after 24 h and 1,000 h at 1000°C (Figure 5b). After 24 h of oxidation, EDS maps indicate the formation of both TiO_2 and Al_2O_3 equiaxed grains. Such a microstructure is typical of the material, it does not result from any damage during the preparation of the sample. One can also distinguish some TiO_2 grains on the external surface of alumina. After 24 h and 1,000 h at 1,000°C, the thickness of the Al_2O_3 layer is equivalent but the Al_2O_3 layer is denser for a longer oxidation time. As a consequence, the low weight gain measured at 1,000°C between 24h and 1,000 h is related to the formation of a thin and dense Al_2O_3 layer. After 1,000 h of oxidation, a few TiO_2 nodules are present at the surface of the Al_2O_3 layer as observed using OM.

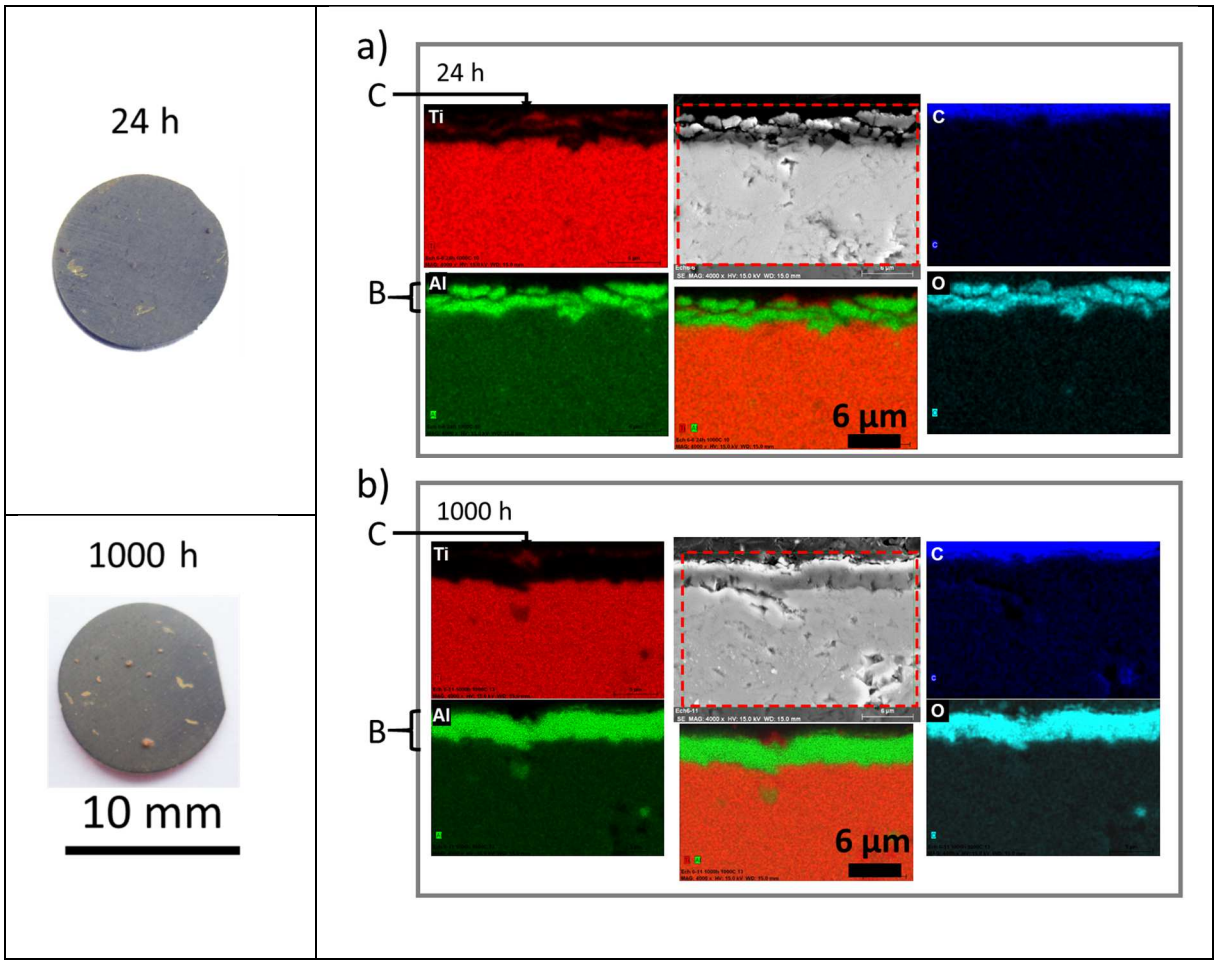

Figure 5: Oxidation tests in ambient air at 1000°C up to 1,000 h performed on different samples densified by SPS at 1315°C/75MPa/2min from heat treated Ti-1.05Al-1.9TiC powder mixtures. On the left, white Light microscopy images of the sample surface oxidized during 24h and 1,000 h at 1000°C. On the right, scanning electron microscopy cross section observation and Ti, Al, C and O corresponding X-Ray maps of the oxide scale after oxidation during 24h (a) and 1,000 h (b) at 1000°C.

Finally, for oxidation temperatures in the range 800-1,000°C, depth composition profiles performed into the MAX phase near the oxide/Ti_3AlC_2 interface confirm the absence of an Al and/or Ti depleted zone.

After oxidation at 900 and 1,000°C, the high-temperature isothermal oxidation resistance of Ti_3AlC_2 is in good agreement with Qian et al. results [18]. As reported in the literature, in the temperature range 900-1,000°C, passivating oxidation is characterized by the formation of a dense Al_2O_3 layer at the surface of the Ti_3AlC_2 phase and, by the existence of TiO_2 nodules at the surface of the Al_2O_3 layer [19-26, 34]. Moreover, the oxide layer displays good adhesion

with the MAX phase substrate. In addition, due to the presumed high mobility of Al atoms through the numerous grain boundaries of the fine-grained Ti_3AlC_2 sample, Al depletion does not occur at the Ti_3AlC_2/Al_2O_3 interface.

In the present study, XRD analyses indicate the growth of the α-Al_2O_3 layer during oxidation at 900°C and 1,000°C. As reported by other authors, such analyses suggest that TiO_2 nodules are formed in the early stages of oxidation. The slow growth of such nodules is related to the slow diffusion of Ti ions through the dense Al_2O_3 layer. Indeed, during the first oxidation stage, oxygen partial pressure at the Ti_3AlC_2/oxidizing atmosphere interface is high allowing the oxidation of both Ti and Al [20]. Once the oxide scale has grown, one can note the existence of an O gradient into the oxide layer which promotes Al oxidation. Indeed, Al_2O_3 being thermodynamically more stable than TiO_2, the O partial pressure required to induce the formation of Al_2O_3 is low as compared to that of TiO_2. Moreover, the crystal structure of Ti_3AlC_2, characterized by weak Ti-Al and C-Al atomic bonds mainly promotes Al diffusion within the grain.

3.2.2. Influence of the Ti_3AlC_2 MAX phase microstructure

3.2.2.1. Grain size effect

The oxidation kinetics of Ti_3AlC_2 MAX phase produced by SPS (Densification of Ti_3AlC_2 powder by SPS at 1315°C/75MPa/2min) and HIP (Simultaneous synthesis and densification at 1450°C/2h and 50MPa/1h) techniques was investigated by thermogravimetric measurements in the temperature range 800-1000°C in synthetic air (Figures 6a and 6b). HIPed specimens have a grain size (mean area in the range 600-4000 μm^2) much larger than the ones measured in the SPSed specimens (mean area about 15 μm^2). As a consequence, HIPed and SPSed

specimens will be further denominated as coarse-grained and fined-grained samples respectively.

First of all, one can observe that oxidation kinetics related to the Ti_3AlC_2 SPSed sample are not consistent with the weight gains obtained using oxidation tests in ambient air in a classical furnace (See Figures 6c). In fact, using TGA analyses in synthetic air, the weight gain increases with the oxidation temperature whereas for oxidation tests in ambient air, the weight gain obtained after 100h of oxidation at 800°C is intermediate between the ones measured at 900°C and 1,000°C. Note that a comparison of the Ti_3AlC_2 weight gain is straightforward since oxidation is sensitive to the atmosphere (ambient air in a resistive furnace, synthetic air in the TGA equipment) but also to the heating and cooling steps (heating and cooling under dry air inside the TGA equipment, sample introduced in the furnace once the oxidation temperature is reached and air-cooled at the end of the test) which are in fact different for both oxidation tests.

For HIPed samples and, similarly to SPSed ones, Figures 6a and 6b show that the weight gain increases with the oxidation temperature and time for oxidation up to 100h under synthetic air in the temperature range 800-1,000°C. By comparing these two figures, one can notice that the weight gains related to the oxidation of the Ti_3AlC_2 samples synthesized by HIP are higher than that obtained from SPS. Indeed, for fine-grained samples the higher weight gains do not exceed 4 g/m^2 after 100 h oxidation whereas such a weight gain is reached after only 5 h at 800°C for coarse-grained samples.

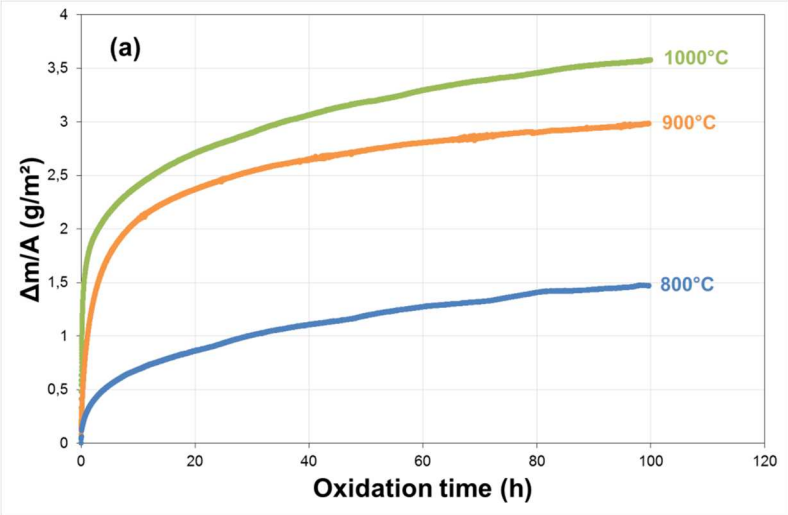

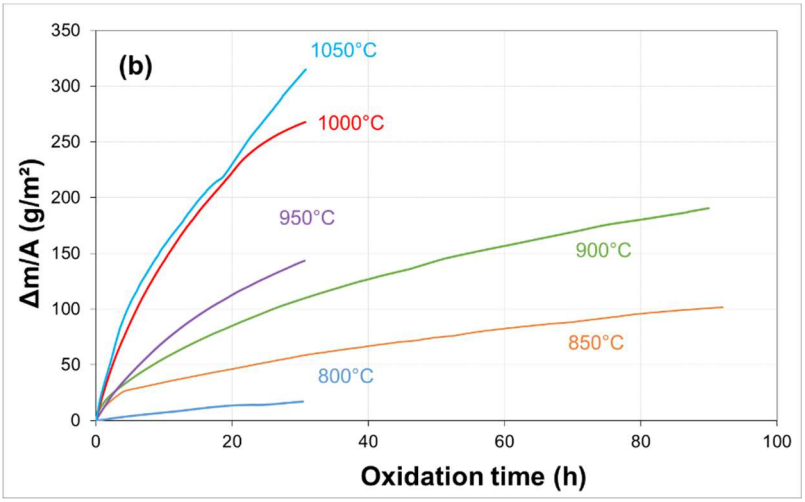

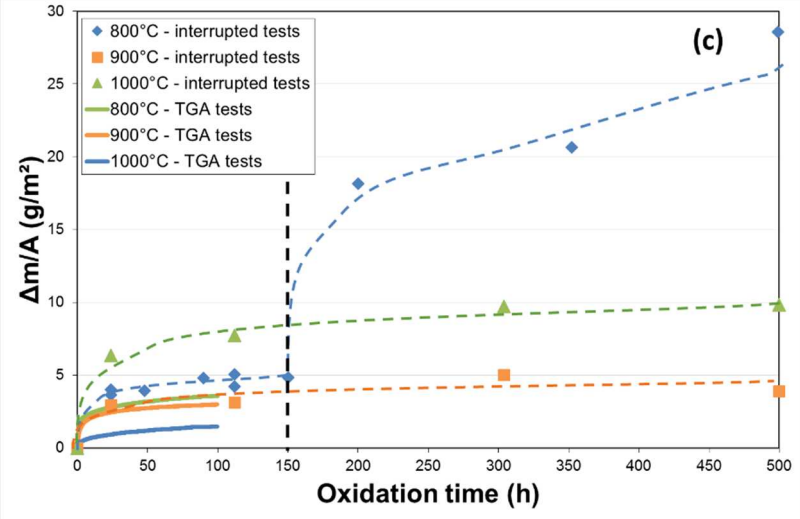

Figure 6: Δm/A plotted as a function of oxidation time, in synthetic air, in the temperature range 800-1000°C. (a) for SPSed samples produced from Ti_3AlC_2 powder densified at 1315°C/75MPa/2min, (b) for HIPed samples produced at 1450°C/2h and 50MPa/1h, (c) for SPSed samples with a comparison between ambient air and TGA oxidation tests.

Figure 7 shows the variation of log(t) as a function of log (Δm/A) for the Ti_3AlC_2 SPSed samples. This representation enables to analyze the oxidation kinetics of the samples. Indeed, if we consider an oxidation law described as a power law such as $\left(\frac{\Delta m}{A}\right)^n = k_n.t$ (with n a kinetics specific exponent and k_n the oxidation constant), the log-log representation allows to assess the n exponent. For n=2, the oxidation kinetics is described by a parabolic law and for n=3, the oxidation kinetics is described by a cubic law. Both kinetics have been used to characterize MAX phases. It has to be noticed that M. W. Barsoum et al. and J. L. Smialek have shown that a cubic law can fit the experimental results better than a parabolic one [27, 28].

In our case, Figure 7 exhibits that neither parabolic nor cubic fit the kinetics observed on Ti_3AlC_2 SPSed samples, excepted at 800°C where cubic kinetics can be applied. Nevertheless, for sake of comparison with other published data, a parabolic law has been chosen to extract the corresponding parabolic rate constants (k_p) and apparent activation energies.

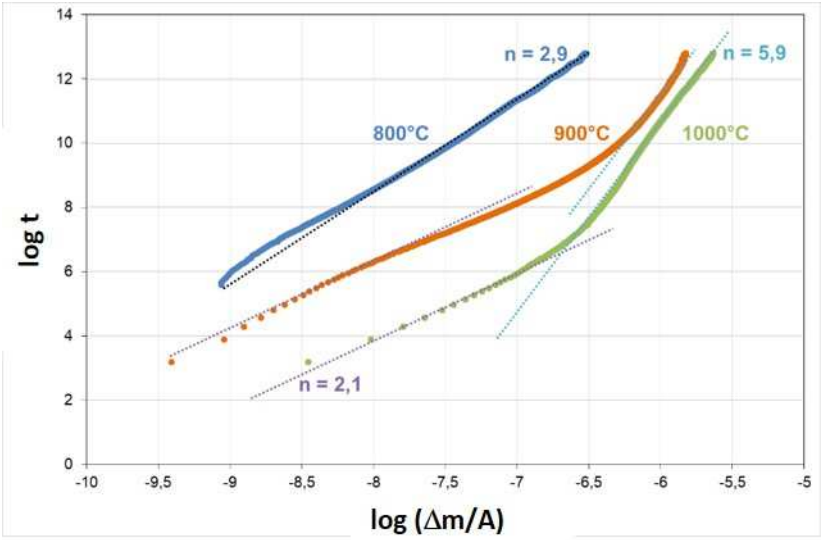

Figure 7: Analysis of the oxidation kinetics of the SPSed specimens (produced from Ti_3AlC_2 powder densified at 1315°C/75MPa/2min) after oxidation in the temperature range 800-1000°C during 100h in synthetic air.

Figure 8 shows the Arrhenius plot of k_p versus the inverse of temperature for the coarse and fine-grained samples. In the two cases, a linear fit is obtained. The slope of the straight line

can refer to activation energy only in cases where the rate-controlling step is well defined, unique and controlled by diffusion through the oxide layer or diffusion to the oxide/air or oxide/MAX phase interfaces. As the properties of the diffusion medium vary with temperature, the effect of this variation also gets incorporated into the variation of rate with temperature, and, consequently, on the apparent activation energy. Thus, the slope of the straight line is merely a temperature coefficient and not the "true" activation energy. The apparent activation energies were evaluated to be 69 and 226 kJ.mol^{-1} for fine and coarse-grained samples respectively. The apparent activation energy determined for the coarse-grained sample lies in the range 136-258 kJ.mol^{-1}, values published previously [21, 26, 32] for Ti_3AlC_2 grains for which the specific grain sizes are not given. Nevertheless, the processing routes used to synthesize the samples for those studies suggest that grains are coarser than the ones obtained in our SPSed samples. Similarly, the apparent activation energy obtained on the fine-grained specimens (69 kJ.mol^{-1}) implies that during the first stages of oxidation, where alumina is mostly formed, mass gain is less temperature dependent.

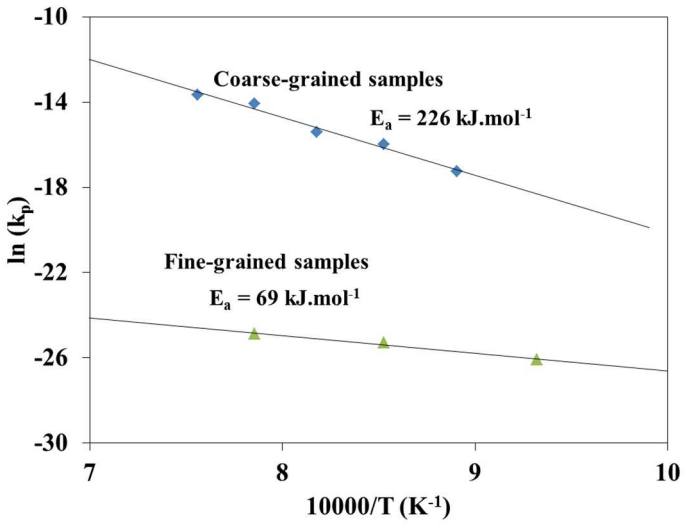

Figure 8: Arrhenius plot of the parabolic rate constant as a function of the inverse temperature for the coarse-grained (diamond) and fine-grained (triangle) specimens.

To investigate the effect of grain size on the oxidation resistance, SEM observations were performed after 30 h of oxidation at 950°C in synthetic air. Figure 9a shows a SEM cross section micrograph of the oxide scale onto the Ti_3AlC_2 MAX phase. Figure 9a reveals the presence of a thick oxide layer (100-170 µm thickness) at the surface of the Ti_3AlC_2 coarse-grained sample. This layer consists of an external TiO_2 layer (light contrast) with some Al_2O_3 grains, an intermediate Al_2O_3 layer (dark contrast) and an internal layer containing both TiO_2 and Al_2O_3. Such a structure is similar to the one observed for the fine-grained Ti_3AlC_2 sample oxidized at 800°C for 500 h in lab air for which a non-protective oxidation process takes place.

Figure 9b shows a representative pore located in the Ti_3AlC_2 phase near the oxidized surface. At the interface between the pore and the surrounding coarse-grained Ti_3AlC_2, the presence of a thin Al_2O_3 layer is noticeable. Moreover, one can observe that some grain boundaries around the pore exhibit lighter chemical contrasts as compared to the MAX phase. X-ray mapping and corresponding EDS analyses performed on these grain boundaries demonstrate that such a contrast corresponds to an Al-depletion. Grain boundaries are thus preferred diffusion paths for aluminum allowing the formation of Al_2O_3 at the interface between the pore and the surrounding coarse-grained MAX phase. Moreover, the diffusion of Al atoms is presumed to be the rate limiting step of the oxidation process at the pore/MAX grains interface. Such a contrast difference is not observed at the grain boundary in fine-grained microstructures. The large number of grain boundaries in fine-grained samples increases the number of diffusion paths for Al atoms which is presumed to improve Al activity at the surface and to enhance Al_2O_3 formation. As a result, alumina is rapidly formed on top of the Ti_3AlC_2 fine-grained surface and it led to a protective oxide scale.

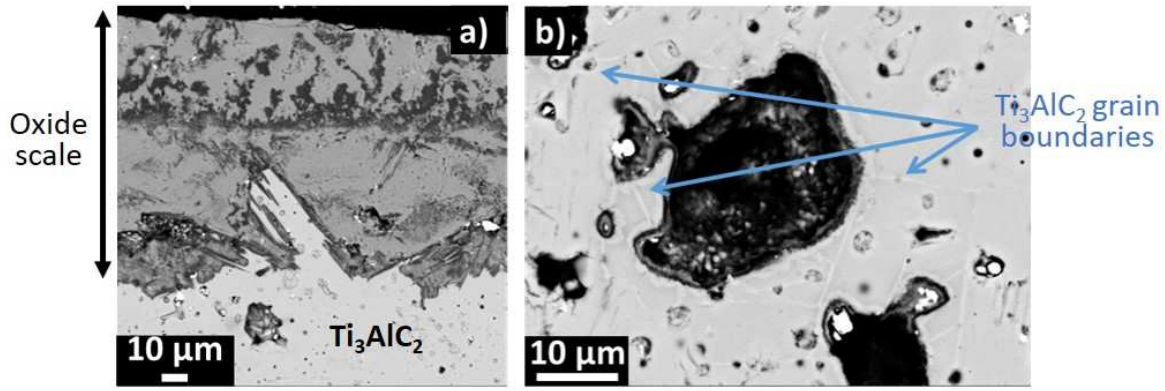

Figure 9: (a) SEM cross section observation of the oxide scale onto the Ti_3AlC_2 MAX phase. (b) SEM cross section observation of the sample microstructure around a pore located in the Ti_3AlC_2 phase near the oxidized surface. Blue arrows show white grain boundaries (see text).

To the authors' knowledge, grain size effect on the oxidation resistance of MAX phases is barely discussed in the open literature. Barsoum et al. [34] did not observe any significative grain size effect on the oxidation of Ti_3SiC_2 MAX phase samples. For large (50-200 µm) and fined-grained (4 µm) samples, weight gains are similar or slightly higher for fine-grained samples after oxidation in the temperature range 1,000-1,200°C and in ambient air [34]. On another system, the conclusions drawn by Li et al. are consistent with our interpretation of results. The authors show that a Cr_7C_3 layer is formed at the Cr_2AlC/Al_2O_3 interface during short-term oxidation of a coarse-grained Cr_2AlC sample, which is not the case for a fined-grained microstructure (~2 µm) and/or after a long oxidation time (> 100 h). Their interpretation based on grain boundary densities is consistent with the fact that external Al^{3+} diffusion towards the oxide layer is lower in the case of coarse-grained versus fine-grained structures. This difference of diffusion kinetics can result in the formation of a pronounced Al-depleted layer at the Cr_2AlC/Al_2O_3 interface, which causes the formation of Cr_7C_3 in the case of coarse-grained Cr_2AlC samples, but not in the fine-grained ones. Consequently, the higher grain boundary density for the fine-grained microstructure promotes Al activity at the surface, leading to the formation of a dense and thick Al_2O_3 layer. In the case of coarse-grained Ti_3AlC_2,

the Al activity is reduced and two different oxides can be formed (TiO_2 and Al_2O_3) due to the limiting step which consists in the diffusion of Al^{3+} ions via grain boundaries; the outward diffusion of Ti^{4+} ions and the inward diffusion of O^{2-} ions leading to the formation of TiO_2 phase.

3.2.2.2. Pore content effect

The oxidation kinetics of Ti_3AlC_2 MAX phase compounds produced by SPS using different processing parameters *(1330°C/60MPa/5min for low porosity sample and 1330°C/30MPa/7min for high-porosity sample)* and exhibiting different pore contents *(1.4 and about 7 vol.% respectively)* but a similar grain size distribution was investigated using thermogravimetric measurements at 800°C in synthetic air (Figure 10). The evolution of the weight gain per unit of surface area as a function of the oxidation time is shown in figure 10 for the two samples.

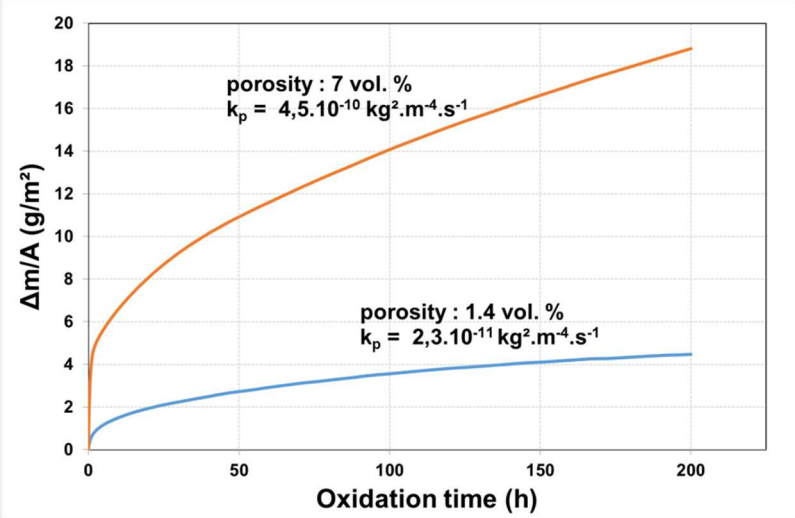

Figure 10: Δm/A plotted as a function of oxidation time at 800°C in synthetic air for SPSed samples with different pore contents. Parabolic rate constant is given. Low and high-porosity samples are produced by SPS densification of Ti_3AlC_2 powder at 1330°C/60MPa/5min and 1330°C/30MPa/7min respectively.

Not surprisingly, weight gain is larger when Ti_3AlC_2 samples exhibit high pore content. Similarly, a parabolic constant was determined for oxidation duration in the range 75-200 h to be about one order of magnitude larger in the case of the high pore content sample (2.3 10^{-13} $g^2.cm^{-4}.s^{-1}$ for 1.4 vol.% of porosity compared to 4.5 10^{-12} $g^2.cm^{-4}.s^{-1}$ for 7 vol.% of porosity). As expected, the growth of the oxide layer is faster in the presence of pores.

To investigate the effect of porosity on oxidation resistance, SEM observations have been performed after 100 h of oxidation in synthetic air at 800°C (Figure 11) and 1,000°C (Figure 12a) on samples exhibiting large pore-networks.

Figure 11 shows SEM cross section observations of such oxidized pore-network whose depth reach several hundred of microns after 100 h of oxidation at 800°C. In its vicinity, oxidation occurs at the grain boundaries (see red arrows in figures 11b and 11c). Grain boundary region, for which internal diffusion of O and external diffusion of Ti and Al are facilitated, are likely connected to the oxidizing atmosphere which promote oxidation. Figures 11b and 11c underline that de-cohesion of MAX-grain boundary is observed (see white arrows). Such a de-cohesion likely results from the development of growth stress at the MAX-grain boundary interface. Furthermore, de-cohesion further allows a fast-diffusion of oxygen into such defect. From EDS analyses, oxidation products are Al_2O_3 and TiO_2, with a main content of Al_2O_3.

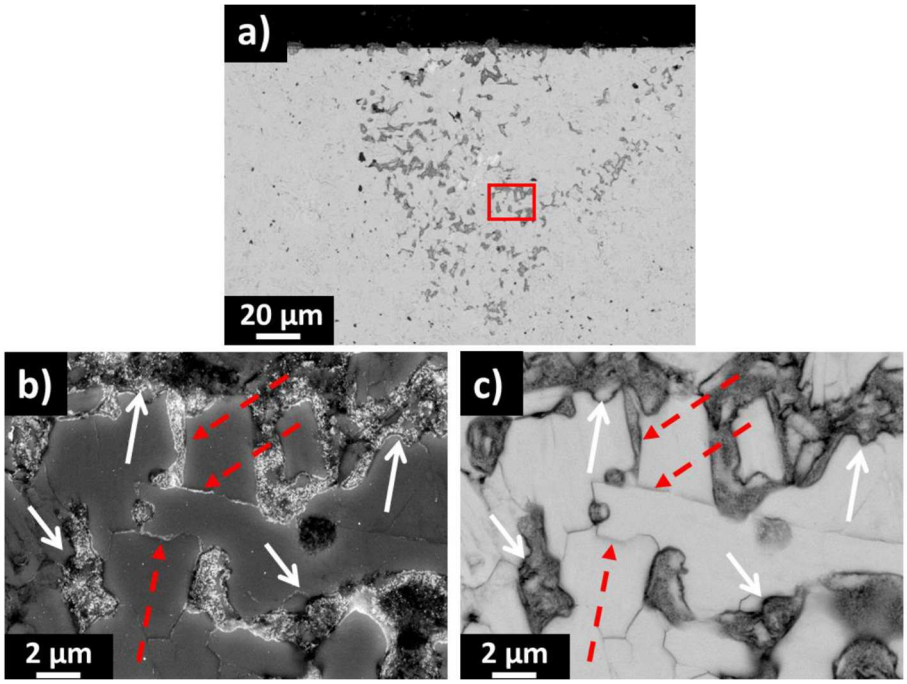

Figure 11: (a) SEM cross section observation of a pore-network region; the oxidization depth reaches several hundred microns after 100 h of oxidation at 800°C. High magnification images obtained in Back-scattered (b) and secondary (c) electron modes. Red arrows show oxidized grain boundary regions whereas white arrows show the de-cohesion of the MAX grain boundary.

Figure 12a shows a pore-network region observed by SEM. Figures 12b and 12d are white light OM observations of the same pore-network region before oxidation. Figures 12c and 12e are polarized light observations of the same pore-network region after 100 h of oxidation at 1,000°C. Polarized light observations (Figures 12c and 12e) show that a large number of TiO_2 nodules have appeared in the pore-network region location. It can also be noticed that, for such oxidation conditions, TiO_2 nodules do no develop in the surrounding areas where Al_2O_3 is the main oxide formed.

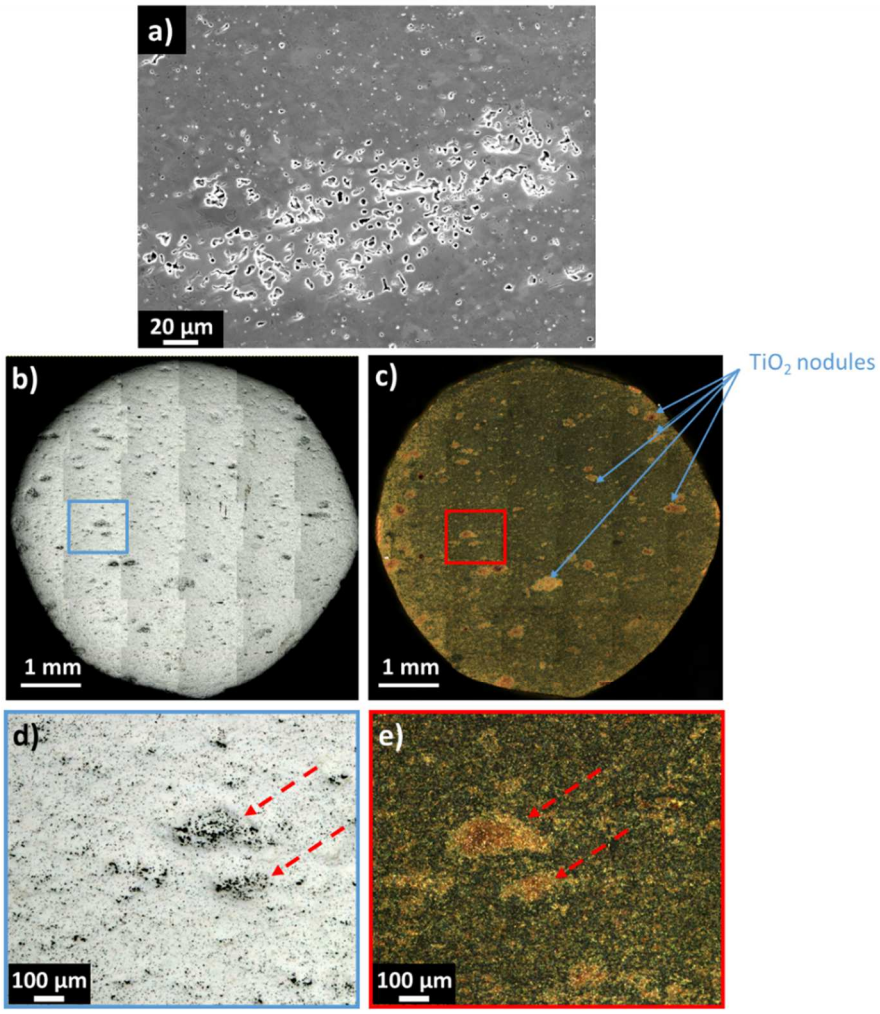

Figure 12: (a) SEM observation of a pore-network region on the sample surface. (b) and (d) white light microscopy images of the same pore-network region before oxidation. (c) and (e) polarized light microscopy images of the same pore-network region after 100 h of oxidation at 1000°C.

From oxidation kinetics and the analysis of oxidation products, our results show that the porosity has a significant effect onto the oxidation resistance of Ti_3AlC_2. Indeed, porous regions lead to the formation of TiO_2 inhibiting the formation of a protective Al_2O_3 layer. Song et al. [40] have reported that sizes of the pores are more determinant than the pore content on the oxidation behavior. Indeed, Song [40] and Tallman [24] have studied crack-healing into Ti_3AlC_2: they have demonstrated that depending on the width of the crack -*which can be assimilated to cavities or porosities*- the oxidation products may vary. Indeed, after 2h

oxidation at 1100°C, densely packed α-Al_2O_3 particles are formed, by inward diffusion of O and outward diffusion of Al, in cracks less than 1µm wide. α-Al_2O_3 particles formed in large cracks are more equiaxed and less densely packed. The absence of columnar particles in cracks or in cavities promotes the external diffusion of Ti ions through the grain boundaries of the equiaxed particles and thus the formation of TiO_2 at the surface of Al_2O_3, in good agreement with the present study.

3.2.2.3. Secondary phase influence

Short-term oxidation tests (10 to 60 min) were performed at 800 and 1,000°C in order to study the oxidation behavior of TiC and Ti_xAl_y inclusions; these secondary phases being frequently formed when Ti_3AlC_2 is synthesized. OM and SEM observations were performed in the same area before and after oxidation to identify the oxides that are formed on top of the secondary phases.

Figure 13a is a white light OM observation of a sample region before oxidation; figure 13b is a SEM observation of the same region after 60 min of oxidation at 800°C. Black areas in figure 13a are either alumina or pores whereas dark grey areas and light grey ones are respectively TiC and Ti_3AlC_2 phases. These figures demonstrate that TiO_2 nodules are preferably formed onto TiC particles. Such a conclusion is also valid for oxidation time in the range 10-60 min and for temperatures equal to 800 or 1,000°C. Moreover, the geometry of the TiO_2 inclusions corresponds very well to the geometry of the initial TiC impurities, without interfering onto the neighboring Ti_3AlC_2 grains. Such a result is in good agreement with other studies [41, 42].

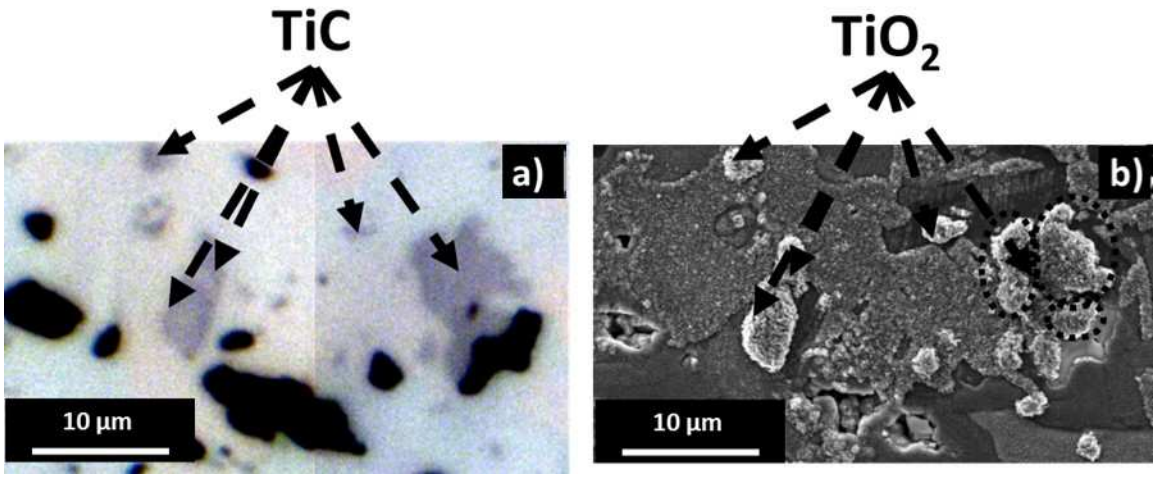

Figure 13: (a) white light OM observation of the SPSed sample produced from Ti_3AlC_2 powder densified at 1315°C/75MPa/2min. Black areas are either alumina or pores whereas dark grey and light grey areas are respectively TiC and Ti_3AlC_2 phases. (b) SEM observation of the same region after 60 min of oxidation at 800°C.

Figure 14a is a white light OM observation of a sample region before oxidation; figure 14b is a SEM observation of the same region after 60 min of oxidation at 800°C. The oxidation of Ti_xAl_y secondary phases (white area in figure 14a and black areas in figure 14b) is very slow compared to that of the TiC particles (see figure 13). Depending on the stoichiometry of the Ti_xAl_y intermetallic, it has been reported that Ti_xAl_y grains may be covered either by a thin Al_2O_3 layer (for Ti_xAl_y enriched in Al) or by a thick Al_2O_3/TiO_2 mixed oxide layer (in the case of Ti_xAl_y enriched in Ti) [43, 44]. These observations also underline that the oxidation kinetics of Ti_3AlC_2 grains could be very different from one to the other. Indeed, some Ti_3AlC_2 grains do not seem oxidized (see continuous circle in figure 14b) whereas some others are oxidized (see dotted circle in figure 14b). Such a feature may be related to the relative orientation of MAX grains with respect to the surface. Indeed, SPSed samples are likely to exhibit a preferential orientation as described by Duan et al. [45] using Cr_2AlC powders. Moreover, the strong crystallographic anisotropy of Ti_3AlC_2 MAX phase suggests that grains orientation may affect

the oxidation properties of the material. Nevertheless, additional work is needed to confirm this assumption.

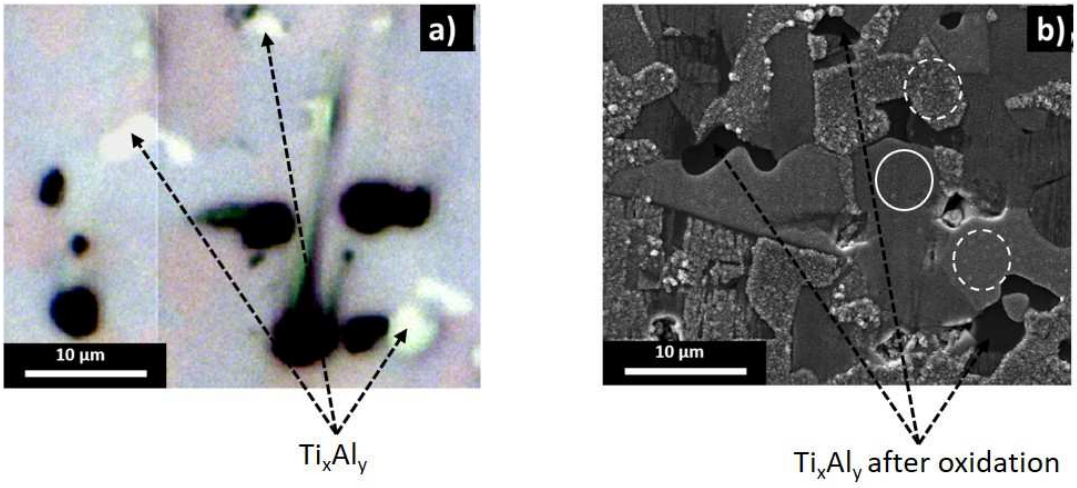

Figure 14: (a) white light OM observation of the SPSed sample produced from Ti_3AlC_2 powder densified at 1315°C/75MPa/2min. Black areas are either alumina or pores whereas light grey and white areas are respectively Ti_3AlC_2 and Ti_xAl_y phases. (b) a SEM observation of the same region after 60 min of oxidation at 800°C.

4. Conclusions

Coarse and fine-grained Ti_3AlC_2 samples were produced respectively by HIP and SPS. It is demonstrated that the oxidation in the 900°C – 1,000°C temperature range of fine-grained samples leads to the formation of a passivating alumina scale whereas the oxidation of coarse-grained samples leads to the formation of a mixed (TiO_2+Al_2O_3) layer which is less protective: the weight gain per area unit being 2 order of magnitude larger at 1,000°C. Such a feature results from the high density of grain boundaries in the fine-grained material which leads to a large number of diffusion paths for Al^{3+} ions. Indeed, Al depleted grain boundaries have been observed after oxidation of the coarse-grained samples.

SPSed samples were synthesized with different pore contents and secondary phase contents. From oxidation kinetics and a fine characterization of oxidation products, it is demonstrated

that porosity has a significant effect onto the oxidation resistance of Ti_3AlC_2. Indeed, regions with a high concentration of pores lead to the formation of TiO_2 inhibiting the formation of a protective Al_2O_3 layer. It is also shown that TiC impurities are rapidly oxidized onto TiO_2 whereas Ti_xAl_y intermetallics seems to be weakly oxidized, at least for short term oxidation conditions lower than 60 min at 1,000°C. Finally, it has also been demonstrated that, for fine-grained samples, the oxide scale does not grow for oxidation time in the range 20-40 days.

Acknowledgements

The authors acknowledge SAFRAN for the financial support and for E. Drouelle PhD grant.

References

[1] W. Jeitschko, H. Nowotny and F. Benesovsky, Kohlen-stoffhaltige ternare Verbindungen (H-Phase), Monatshefte für Chemie, 94, 4, (1963) 672-676.

[2] V.H. Nowotny, Strukturchemie einiger Verbindungen der Übergangsmetalle mit den elementen C, Si, Ge, Sn, Prog. Solid State Chem. 5 (1971) 27–70.

[3] J. L. Smialek, J.A. Nesbitt, T.P. Gabb, A. Garg, R.A. Miller, Hot corrosion and low cycle fatigue of a Cr_2AlC-coated superalloy, Mat. Sc. and Eng. A, 711 (2018) 119.

[4] J. L. Smialek, and S. Gray, Type II Hot Corrosion Screening Tests of a Cr_2AlC MAX Phase Compound, Oxid. Met., 90 (2018) 555-570.

[5] M. Sokol, J. Yang, H. Keshavan, M. W.Barsoum, Bonding and oxidation protection of Ti_2AlC and Cr_2AlC for a Ni-based superalloy, J. of Eur. Ceram. Soc., 39 (2019) 878-882.

[6] J. L. Smialek, Oxidation of Al_2O_3 Scale-Forming MAX Phases in Turbine Environments, Met. Mat. Trans., 49, 3 (2018) 782.

[7] D.J. Tallman, M. Naguib, B. Anasori, M.W. Barsoum, Tensile creep of Ti_2AlC in air in the temperature range 1000–1150°C, Scr. Mater. 66 (2012) 805–808.

[8] M. Radovic, M.W. Barsoum, T. El-Raghy, S.M. Wiederhorn, Tensile creep of fine grained (3–5 μm) Ti_3SiC_2 in the 1000–1200°C temperature range, Acta Mater. 49 (2001) 4103–4112.

[9] M. Radovic, M.W. Barsoum, T. El-Raghy, S.M. Wiederhorn, Tensile creep of coarse-grained Ti_3SiC_2 in the 1000–1200°C temperature range, J. of Alloys and Compounds, 361 (2003) 299–312.

[10] E. Drouelle, A. Joulain, V. Gauthier-Brunet, P. Villechaise, P. Sallot and S. Dubois, Deformation mechanisms during high temperature tensile creep of Ti_3AlC_2 MAX phase, J. of Alloys and Compounds, 693 (2017) 622-630.

[11] M. W. Barsoum, N. Tzenov, A. Procopio, T. El-Raghy, and M. Ali, Oxidation of $Ti_{n+1}AlX_n$ (n=1-3 and X=C, N): II. Experimental Results." Journal of The Electrochemical Society, 148, 8 (2001) C551.

[12] D. B. Lee and S. W. Park, High-Temperature Oxidation of Ti_3AlC_2 between 1173 and 1473K in Air, Materials Science and Engineering A 434, 1–2 (2006) 147-154.

[13] G. M. Song, Y. T. Pei, W. G. Sloof, S. B. Li, J. Th. M. De Hosson, and S. Van der Zwaag, Early Stages of Oxidation of Ti_3AlC_2 Ceramics, Materials Chemistry and Physics, 112, 3 (2008) 762-768.

[14] T. Ai, High-Temperature Oxidation Behavior of Un-Dense Ti_3AlC_2 Material at 1000°C in Air, Ceramics International, 38, 3 (2012) 2537–2541.

[15] H. P. Zhu, X. K. Qian, H. Y. Wu, J. Lei, Y. C. Song, X. D. He, and Y. Zhou, Cyclic Oxidation of Ternary Layered Ti_2AlC at 600-1000°C in Air, International Journal of Applied Ceramic Technology, 12 (2015) 403-410.

[16] X. Li, L. Zheng, Y. H. Qian, J. Xu, and M. S. Li, Breakaway Oxidation of Ti_3AlC_2 during Long-Term Exposure in Air at 1100°C, Corrosion Science 104 (2016) 112–22.

[17] X. C. Li, Y. H. Qian, L. Zheng, J. J. Xu, and M. S. Li, Determination of the Critical Content of Al for Selective Oxidation of Ti_3AlC_2 at 1100°C, Journal of the European Ceramic Society, 36, 14 (2016) 3311–18.

[18] X. K. Qian, X. D. He, Y. B. Li, Y. Sun, H. Li, and D. L. Xu, Cyclic Oxidation of Ti_3AlC_2 at 1000-1300°C in Air, Corrosion Science, 53, 1 (2011) 290–95.

[19] G. M. Song, V. Schnabel, C. Kwakernaak, S. van der Zwaag, J. M. Schneider, and W. G. Sloof, High Temperature Oxidation Behaviour of Ti_2AlC Ceramic at 1200°C, Materials at High Temperatures, 29, 3 (2012) 205–209.

[20] X. H. Wang, and Y. C. Zhou, High-Temperature Oxidation Behavior of Ti_2AlC in Air, Oxidation of Metals, 59, 3–4 (2003) 303-320.

[21] X. W. Xu, Y. Li, B. C. Mei, J. Q. Zhu, H. Liu, and J. Qu, Study on the Isothermal Oxidation Behavior in Air of Ti_3AlC_2 Sintered by Hot Pressing, Science in China Series E: Technological Sciences, 49, 5 (2006) 513-520.

[22] X. W. Xu, Y. X. Li, J. Q. Zhu, and B. C. Mei, High-Temperature Oxidation Behavior of Ti_3AlC_2 in Air, Transactions of Nonferrous Metals Society of China, 16 (2006) s869-s873.

[23] X. H. Wang and Y. C. Zhou, Synthesis and Oxidation of Bulk Ti_3AlC_2, Key Engineering Materials, 224-226 (2002) 785-790.

[24] D. J. Tallman, B. Anasori and M. W. Barsoum, A Critical Review of the Oxidation of Ti_2AlC, Ti_3AlC_2 and Cr_2AlC in Air, Materials Research Letters, 1, 3 (2013) 115-125.

[25] J. L. Smialek, Kinetic Aspects of Ti_2AlC MAX Phase Oxidation, Oxidation of Metals, 83, 3–4 (2015) 351-366.

[26] X. H. Wang and Y. C. Zhou, Oxidation Behavior of Ti_3AlC_2 at 1000–1400°C in Air, Corrosion Science, 45, 5 (2003) 891–907.

[27] S.B. Li, X. D. Chen, Y. Zhou, and G. M. Song, Influence of Grain Size on High Temperature Oxidation Behavior of Cr_2AlC Ceramics, Ceramics International, 39, 3 (2013) 2715-2721.

[28] J. Gonzalez-Julian, T. Go, D. E. Vassen, Thermal cycling testing of TBCs on Cr_2AlC MAX phase substrates, , 340 (2018) 17 – 24.

[29] J. Gonzalez-Julian, S. Onrubia, M. Bram, C. Broeckmann, R. Vassen, O. Guillon, High temperature oxidation and compressive strength of Cr_2AlC MAX phase foams with controlled porosity**,** Journal of the American Ceramic Society**,** 101 (2017) 11-12.

[30] J. L. Smialek, Unusual Oxidative Limitations for Al-MAX Phases, NASA Report/TM-2017-219444.

[31] J. Gonzalez-Julian, T. Go, D.E. Mack, R. Vaßen, Environmental resistance of Cr_2AlC MAX phase under thermal gradient loading using a burner rig, J. of Am. Ceram. Soc., 101 (2018) 1841-1846.

[32] X. H. Wang and Y. C. Zhou, Oxidation Behavior of TiC-Containing Ti_3AlC_2 Based Material at 500-900 °C in Air, Materials Research Innovations, 7, 6 (2003) 381-390.

[33] W. K. Pang, I. M. Low, B. H. O'Connor, Z. M. Sun, and K. E. Prince, Oxidation Characteristics of Ti_3AlC_2 over the Temperature Range 500–900°C, Materials Chemistry and Physics, 117, 2–3 (2009) 384-389.

[34] M. W. Barsoum, L. H. Ho-Duc, M. Radovic, and T. El-Raghy, Long Time Oxidation Study of Ti_3SiC_2, Ti_3SiC_2/SiC, and Ti_3SiC_2/TiC Composites in Air, Journal of the Electrochemical Society 150, 4 (2003) B166.

[35] G. P. Bei, PhD thesis, Université de Poitiers, Synthesis, microstructural characterization and mechanical properties of nanolaminated $Ti_3Al_xSn_{(1-x)}C_2$ MAX phases, 2011.

[36] S. Dubois, G. P. Bei, C. Tromas, V. Gauthier-Brunet and P. Gadaud, Synthesis, microstructure and mechanical properties of $Ti_3Sn_{(1-x)}Al_xC_2$ MAX phase solid solutions. Intern. J. of Applied Ceramic Techn. 7, 6 (2010) 719-729

[37] G. P. Bei, V. Gauthier-Brunet, C. Tromas and S. Dubois, Synthesis, characterization and intrinsic hardness of layered nanolaminate Ti_3AlC_2 and $Ti_3Al_{0.8}Sn_{0.2}C_2$ solid solution, J. of the Am. Ceram. Soc., 95 (1) 102 (2012).

[38] E. Drouelle, PhD thesis, Relations microstructure, propriétés mécaniques et résistance à l'oxydation de la phase MAX Ti_3AlC_2, Université de Poitiers, 2017.

[39] F. Naimi, PhD thesis, Scientific and technological approaches for sintering and joining of metallic materials by SPS, Université de Dijon, 2013.

[40] G. M. Song, Y. T. Pei, W. G. Sloof, S. B. Li, J. T. M. De Hosson, and S. Van der Zwaag, Oxidation-Induced Crack Healing in Ti_3AlC_2 Ceramics, Scripta Materialia, 58 (1) (2008) 13–16.

[41] N. F. Macdonald and C. E. Ransley, The Oxidation of Hot-Pressed Titanium Carbide and Titanium Boride in the Temperature Range 300°–1000° C, Powder Metallurgy, 2, 3 (1959) 172-176.

[42] V. B. Voitovich, Mechanism of the High Temperature Oxidation of Titanium Carbide, High Temperature Materials and Processes, 16, 4, (1997) 243-254.

[43] J. L. Smialek and D. L. Humphrey, Oxidation Kinetics of Cast $TiAl_3$, Scripta Metallurgica et Materiala, 26, 11 (1992) 1763–68.

[44] J. L. Smialek and N. Jacobson, Oxidation of High-Temperature Aerospace Materials, in High Temperature Materials and Mechanisms edited by Yoseph Bar-Cohen, CRC Press, (2014) pp. 95–162.

[45] X. M. Duan, L. Shen, D. Jia, Y. Zhou, S. Van der Zwaag, and W. G. Sloof, Synthesis of High-Purity, Isotropic or Textured Cr_2AlC Bulk Ceramics by a Two-Step Sintering Process, J. of Eur. Ceram. Soc., 35 (2015) 1393-1400.